LQ Covariance Control with Deadline Constraint and Frobenius Terminal Loss

Tushar Sial* and Abhishek Halder†
Department of Aerospace Engineering, Iowa State University, Ames, IA 50011, USA

This work advances the state-of-the-art for optimal control of the state covariance for a continuous-time stochastic linear time-varying control system. Specifically, we formulate and solve the fixed horizon linear quadratic covariance steering problem in continuous time, in which a time-varying linear state-feedback controller is optimized to steer the system state covariance close to a desired terminal value. The resulting optimality conditions yield a coupled matrix ODE two-point boundary value problem, which we solve via a novel matricial recursive algorithm and prove its convergence. The algorithm's analysis leverages linear fractional transforms parameterized by the state transition matrix of the associated Hamiltonian. The computational tractability of the resulting control algorithm has several applications across diverse domains, such as robotic tracking and autonomous rendezvous and docking missions for satellites. To illustrate the results, the proposed algorithm is tested and validated for a close-proximity rendezvous scenario by modeling the relative motion of a service spacecraft with a target satellite in low Earth orbit using the Clohessy–Wiltshire equations with stochastic disturbances.

I. Introduction

The problem of steering the state covariance* $\boldsymbol{\Sigma}_t$ to a target covariance $\boldsymbol{\Sigma}_d$ was originally motivated [1] by treating $\boldsymbol{\Sigma}_d$ as a statistical performance specification. This perspective has proven particularly useful in aerospace guidance and navigation, where mission requirements on performance are naturally cast as covariance steering problems [2–5].

The initial uncertainty is encoded in the covariance $\boldsymbol{\Sigma}_0$, which is typically provided by an estimator. A terminal cost $\phi\left(\boldsymbol{\Sigma}_1, \boldsymbol{\Sigma}_d\right)$ enables the control designer to balance the penalty for mismatch in terminal second-order statistics against the average cost-to-go $\int_{t_0}^{t_1} \mathbb{E}\left(\|\boldsymbol{u}_t\|_2^2 + \boldsymbol{x}_t^\top \boldsymbol{Q}_t \boldsymbol{x}_t\right) \mathrm{d}t$.

The terminal cost 2 is chosen for its simplicity relative to alternatives such as (3). Although the optimality conditions for the terminal cost (3) were derived in [6], a dedicated numerical algorithm for that more general setting has yet to be developed. By focusing on the simpler terminal cost (2), this work proposes a provably convergent numerical algorithm for solving problem (1). From a geometric standpoint, the terminal cost (2) is Euclidean in nature, as it does not account for the Riemannian structure [7, Ch. 6] of the cone of positive definite covariance matrices. Nevertheless, the design and convergence analysis of the proposed algorithm reveal considerable subtlety, and represent a meaningful advance in the numerical solution of this class of problems.

In the *discrete-time* setting, a growing body of literature [8–13] has addressed fixed-horizon LQ covariance steering problems with terminal cost. In these works, the terminal cost ϕ is typically taken as the squared Bures-Wasserstein metric (3) or its unregistered counterpart, the Gromov-Wasserstein metric [14, 15]. In the *continuous-time* setting, fixed-horizon covariance steering with terminal cost remains comparatively underexplored. The pioneering work [6] studied the fixed-horizon LQ covariance steering problem with the Bures-Wasserstein terminal cost and derived the associated optimality conditions. While the computation therein relied on a shooting method, a more principled and systematic algorithm for the same has not been established. More recently, [16] derived optimality conditions for the general nonlinear non-Gaussian variant of this problem with the Wasserstein terminal cost, expressed as forward-backward stochastic differential equations, though the numerical solution of these conditions was not investigated.

The main reason for this imbalance in the literature between discrete-time and continuous-time formulations is computational difficulty. The discrete-time LQ covariance steering with terminal cost naturally leads to semi-definite programming and is therefore amenable to off-the-shelf interior-point solvers. In contrast, the continuous-time LQ

*Graduate Research Assistant, Department of Aerospace Engineering, Iowa State University, AIAA Student Member 1859372; tsial@iastate.edu.

†Associate Professor, Department of Aerospace Engineering, Iowa State University; ahalder@iastate.edu.

*i.e., the covariance of the controlled state $\boldsymbol{x}_t \in \mathbb{R}^n$ at time $t \in [t_0, t_1]$

covariance steering with terminal cost leads to a coupled nonlinear system of matricial ODEs, and it is not obvious what the principled algorithmic approach is to solve the same.

We propose a computationally efficient solution strategy for the fixed horizon linear quadratic covariance steering problem in continuous time with a Frobenius terminal loss function. Rather than directly tackling the coupled matrix ODE two-point boundary value problem that arises from the necessary conditions of optimality, we develop a symmetric matrix-valued recursive algorithm that exploits the inherent structure of the coupled matrix equations. This paper emphasizes the intuition, structure, and practical implementation of the proposed approach, with rigorous derivations deferred to [17]. The effectiveness of the method is demonstrated through numerical examples on a noisy double-integrator system and a close-proximity orbital rendezvous problem.

The remainder of this paper is organized as follows. Sec. II presents the problem formulation and the optimality conditions as a matricial boundary value problem in the state covariance and its costate, followed by a change of variables that yields a Riccati-Riccati system of matrix ODE boundary value problems. Sec. III introduces three matrix-valued mappings and analyzes their properties, which form the foundation of the recursive algorithm proposed in Sec. IV for solving the system. Sec. V presents numerical examples to demonstrate the proposed method, and Sec. VI concludes the paper.

II. Optimal Covariance Steering

A. Problem Formulation

We consider the following continuous-time linear quadratic (LQ) covariance steering problem:

$$\inf_{\boldsymbol{u}_t \in \mathcal{U}} \phi\left(\boldsymbol{\Sigma}_1, \boldsymbol{\Sigma}_d\right) + \int_{t_0}^{t_1} \mathbb{E}\left(\|\boldsymbol{u}_t\|_2^2 + \boldsymbol{x}_t^\top \boldsymbol{Q}_t \boldsymbol{x}_t\right) \mathrm{d}t \tag{1a}$$

subject to

$$\mathrm{d}\boldsymbol{x}_t = \boldsymbol{A}_t \boldsymbol{x}_t \, \mathrm{d}t + \boldsymbol{B}_t \boldsymbol{u}_t \, \mathrm{d}t + \boldsymbol{B}_t \, \mathrm{d}\boldsymbol{w}_t, \tag{1b}$$

$$\boldsymbol{x}_0 := \boldsymbol{x}(t = t_0) \sim \rho_0 := \mathcal{N}\left(\boldsymbol{0}, \boldsymbol{\Sigma}_0\right), \rho_d := \mathcal{N}\left(\boldsymbol{0}, \boldsymbol{\Sigma}_d\right), \tag{1c}$$

where the time horizon is finite and fixed as $[t_0, t_1]$, the symbol $\mathbb{E}$ denotes the expectation w.r.t. the state vector $\boldsymbol{x}_t \in \mathbb{R}^n$, the $\mathcal{N}$ denotes multivariate normal probability density function (PDF), and $\sim$ is a shorthand for "follows the distribution". In (1c), the ρ_0 is the PDF for the initial state $\boldsymbol{x}_0$, and the ρ_d is the desired PDF for the terminal state at $t = t_1$. Depending on the choice of control policy, the statistics of the controlled terminal state $\boldsymbol{x}_1 := \boldsymbol{x}(t = t_1)$ may not match the desired terminal statistics ρ_d.

In (1a), $\boldsymbol{\Sigma}_1$ is the covariance of the terminal state $\boldsymbol{x}_1 := \boldsymbol{x}(t = t_1)$, which depends on the choice of control policy. The terminal cost ϕ is a measure of error between the terminal state covariance $\boldsymbol{\Sigma}_1$ and a desired state covariance $\boldsymbol{\Sigma}_d$. While many choices for ϕ are possible, in this work, we fix ϕ to be the squared Frobenius or Hilbert-Schmidt norm:

$$\phi\left(\boldsymbol{\Sigma}_1, \boldsymbol{\Sigma}_d\right) := \frac{1}{2}\|\boldsymbol{\Sigma}_1 - \boldsymbol{\Sigma}_d\|_{\text{Frobenius}}^2 = \frac{1}{2}\langle \boldsymbol{\Sigma}_1 - \boldsymbol{\Sigma}_d, \boldsymbol{\Sigma}_1 - \boldsymbol{\Sigma}_d \rangle = \frac{1}{2}\text{trace}\left(\boldsymbol{\Sigma}_1 - \boldsymbol{\Sigma}_d\right)^2 \tag{2}$$

wherein the Hilbert-Schmidt inner product $\langle \boldsymbol{M}, \boldsymbol{N} \rangle := \text{trace}\left(\boldsymbol{M}^\top \boldsymbol{N}\right)$. The prior work [6] considered LQ covariance steering with ϕ as the squared Bures-Wasserstein distance metric [18] between $\boldsymbol{\Sigma}_1, \boldsymbol{\Sigma}_d$, given by

$$\frac{1}{2}\text{trace}\left(\boldsymbol{\Sigma}_1 + \boldsymbol{\Sigma}_d - 2\left(\boldsymbol{\Sigma}_1^{\frac{1}{2}} \boldsymbol{\Sigma}_d \boldsymbol{\Sigma}_1^{\frac{1}{2}}\right)^{\frac{1}{2}}\right), \tag{3}$$

where the exponent $\frac{1}{2}$ denotes principal square root. The metric (3) originates from the theory of optimal transport [19, 20]. If $\boldsymbol{\Sigma}_1, \boldsymbol{\Sigma}_d$ commute (e.g., when the state dimension $n = 1$), then (3) reduces to the squared Fréchet distance [21] $\frac{1}{2}\|\sqrt{\boldsymbol{\Sigma}}_1 - \sqrt{\boldsymbol{\Sigma}}_d\|_{\text{Frobenius}}^2$. Intuitively, the terminal cost ϕ penalizes the mismatch between the second-order statistics of the controlled terminal state $\boldsymbol{x}_1$ from that of a desired state. In this sense, $\boldsymbol{\Sigma}_d$ can be interpreted as a desired statistical tolerance for control performance at $t = t_1$.

The set of admissible control inputs

$$\mathcal{U} := \left\{ \boldsymbol{u} : [t_0, t_1] \times \mathbb{R}^n \mapsto \mathbb{R}^m \mid \mathbb{E}_\rho\left\{\int_{t_0}^{t_1} \|\boldsymbol{u}\|_2^2 \mathrm{d}t\right\} < \infty \forall \rho : \mathbb{R}^n \mapsto \mathbb{R}_{\geq 0}, \int_{\mathbb{R}^n} \rho \, \mathrm{d}\boldsymbol{x} = 1, \int_{\mathbb{R}^n} \|\boldsymbol{x}\|_2^2 \rho \, \mathrm{d}\boldsymbol{x} < \infty \right\}$$

in (1a) comprises adapted finite energy control policies such that (1b) has a strong solution.

In the controlled Itô diffusion (1b), the standard Wiener process $\boldsymbol{w}_t \in \mathbb{R}^m$. We take the same $\boldsymbol{B}_t$ as the control and the noise coefficients, i.e., assume that the input and the noise channels are identical. This is indeed common in practice, e.g., when the noise is due to stochastic actuation, or when the noise enters through external force/torque/current. In (1c), the initial state PDF ρ_0 and the desired terminal sate PDF ρ_d are centered multivariate normals with prescribed covariances $\boldsymbol{\Sigma}_0, \boldsymbol{\Sigma}_d$, respectively.

With Φ as in (2), we make the following assumptions about the data for problem (1).

A1. The pair $(\boldsymbol{A}_t, \boldsymbol{B}_t)$ is bounded and continuous w.r.t. $t \in [t_0, t_1]$, and is uniformly controllable[†].

A2. The state cost-to-go weights $\boldsymbol{Q}_t \succeq \boldsymbol{0}$ for all $t \in [t_0, t_1]$.

A3. The covariances $\boldsymbol{\Sigma}_0, \boldsymbol{\Sigma}_d \succ \boldsymbol{0}$.

We wish to design a linear feedback controller

$$\boldsymbol{u}_t = \boldsymbol{K}_t \boldsymbol{x}_t \tag{4}$$

with deterministic time-varying gain $\boldsymbol{K}_t : [t_0, t_1] \mapsto \mathbb{R}^{m\times n}$, so as to steer the state covariance from $\boldsymbol{\Sigma}_0$ at $t = t_0$, to a neighborhood of $\boldsymbol{\Sigma}_d$ at $t = t_1$, that is optimal w.r.t. (1).

Note that the zero mean assumptions for ρ_0, ρ_d are without loss of generality, since non-zero means can be tackled by adding a time-varying affine term to (4), and separately designing a controller for the same (see [17, Remark 1]).

B. Conditions of Optimality

From (1b) and (4), the controlled state $\boldsymbol{x}_t \sim \mathcal{N}(\boldsymbol{0}, \boldsymbol{\Sigma}_t)$ with covariance dynamics

$$\dot{\boldsymbol{\Sigma}}_t = (\boldsymbol{A}_t + \boldsymbol{B}_t\boldsymbol{K}_t)\,\boldsymbol{\Sigma}_t + \boldsymbol{\Sigma}_t\,(\boldsymbol{A}_t + \boldsymbol{B}_t\boldsymbol{K}_t)^\top + \boldsymbol{B}_t\boldsymbol{B}_t^\top \tag{5}$$

on $\mathbb{S}^n_{++}$, the cone of positive definite matrices. The quadratic objective (1a), then allows us to view $\boldsymbol{\Sigma}_t \in \mathbb{S}^n_{++}$ itself as the state, and define $\boldsymbol{P}_t \in \mathbb{S}^n$ (the affine set of $n \times n$ real symmetric matrices) as the costate. Under the linear state-feedback control law (4) and the assumptions **A1**-**A3**, applying Pontryagin's minimum principle to the Hamiltonian of the covariance steering problem (1) at optimality(refer to [17, Proposition 1] for proof) leads to a coupled ODE boundary value problem on the cotangent bundle $\mathcal{T}^*\mathbb{S}^n_{++} = \mathbb{S}^n_{++} \times \mathbb{S}^n$ in unknown $\left(\boldsymbol{\Sigma}_t^{\text{opt}}, \boldsymbol{P}_t^{\text{opt}}\right)$, given by

$$\begin{aligned}
\dot{\boldsymbol{\Sigma}}_t^{\text{opt}} &= \left(\boldsymbol{A}_t - \boldsymbol{B}_t\boldsymbol{B}_t^\top\boldsymbol{P}_t^{\text{opt}}\right)\boldsymbol{\Sigma}_t^{\text{opt}} \\
&\quad + \boldsymbol{\Sigma}_t^{\text{opt}}\left(\boldsymbol{A}_t - \boldsymbol{B}_t\boldsymbol{B}_t^\top\boldsymbol{P}_t^{\text{opt}}\right)^\top + \boldsymbol{B}_t\boldsymbol{B}_t^\top, && \text{(6a)}\\
-\dot{\boldsymbol{P}}_t^{\text{opt}} &= \boldsymbol{A}_t^\top\boldsymbol{P}_t^{\text{opt}} + \boldsymbol{P}_t^{\text{opt}}\boldsymbol{A}_t - \boldsymbol{P}_t^{\text{opt}}\boldsymbol{B}_t\boldsymbol{B}_t^\top\boldsymbol{P}_t^{\text{opt}} + \boldsymbol{Q}_t, && \text{(6b)}\\
\boldsymbol{\Sigma}_0 &\succ \boldsymbol{0} \quad \text{given}, && \text{(6c)}\\
\boldsymbol{P}_1^{\text{opt}} &= \boldsymbol{\Sigma}_1^{\text{opt}} - \boldsymbol{\Sigma}_d, \quad \boldsymbol{\Sigma}_d \succ \boldsymbol{0} \quad \text{given}. && \text{(6d)}
\end{aligned}$$

The associated optimal gain

$$\boldsymbol{K}_t^{\text{opt}} = -\boldsymbol{B}_t^\top\boldsymbol{P}_t^{\text{opt}}, \tag{7}$$

and the optimal control $\boldsymbol{u}_t^{\text{opt}} = \boldsymbol{K}_t^{\text{opt}}\boldsymbol{x}_t$.

Remark 1. *Direct numerical solution of* (6) *is problematic. At the ODE level, even though* (6b) *is decoupled,* (6a) *is coupled. At the boundary condition level, even though* (6c) *is decoupled,* (6d) *is coupled.*

To circumvent the computational difficulty mentioned above, we make use of the following change-of-variable proposed in [22, 23]:

$$\boldsymbol{H}_t := \boldsymbol{\Sigma}_t^{-1} - \boldsymbol{P}_t \qquad \forall t \in [t_0, t_1]. \tag{8}$$

The works in [22, 23] considered the case where the terminal state covariance $\boldsymbol{\Sigma}_1^{\text{opt}}$ was prescribed as problem data. However, in our setting, neither $\boldsymbol{\Sigma}_1^{\text{opt}}$ nor $\boldsymbol{P}_1^{\text{opt}}$ is known. Only their linear combination is constrained by (6d). Because of this transversality constraint, it is not obvious what, if any, computational benefit may be reaped from (8).

[†]i.e., the controllability Gramian is strictly positive definite $\forall [s, t] \subseteq [t_0, t_1]$.

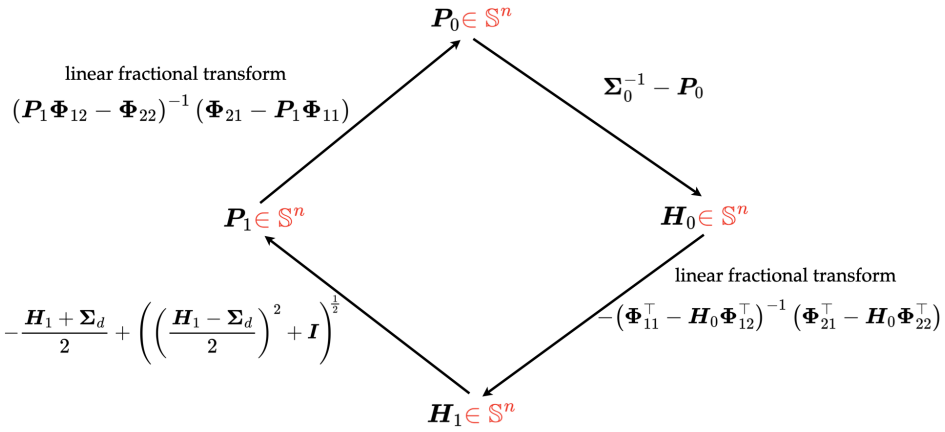

Fig. 1 The proposed fixed point recursion $P_0 \mapsto (P_0)_{\text{next}}$ as a composition of four mappings.

The change-of-variable (8) allows us to set up a system of equations that folds in (8) with the ODEs for $\boldsymbol{P}_t, \boldsymbol{H}_t \in \mathbb{S}^n$ (refer to [17, Proposition 2] for proof). We are now led to solve the coupled nonlinear system of equations:

$$-\dot{\boldsymbol{P}}_t^{\text{opt}} = \boldsymbol{A}_t^\top \boldsymbol{P}_t^{\text{opt}} + \boldsymbol{P}_t^{\text{opt}} \boldsymbol{A}_t - \boldsymbol{P}_t^{\text{opt}} \boldsymbol{B}_t \boldsymbol{B}_t^\top \boldsymbol{P}_t^{\text{opt}} + \boldsymbol{Q}_t, \tag{9a}$$

$$-\dot{\boldsymbol{H}}_t = \boldsymbol{A}_t^\top \boldsymbol{H}_t + \boldsymbol{H}_t \boldsymbol{A}_t + \boldsymbol{H}_t \boldsymbol{B}_t \boldsymbol{B}_t^\top \boldsymbol{H}_t - \boldsymbol{Q}_t, \tag{9b}$$

$$\boldsymbol{H}_0 = \boldsymbol{\Sigma}_0^{-1} - \boldsymbol{P}_0, \tag{9c}$$

$$\boldsymbol{H}_1 \overset{(6d),(8)}{=} (\boldsymbol{P}_1 + \boldsymbol{\Sigma}_d)^{-1} - \boldsymbol{P}_1, \tag{9d}$$

where $\boldsymbol{P}_0 := \boldsymbol{P}_{t=t_0}^{\text{opt}}$, $\boldsymbol{P}_1 := \boldsymbol{P}_{t=t_1}^{\text{opt}}$.

Since $\boldsymbol{\Sigma}_0, \boldsymbol{\Sigma}_d \succ \boldsymbol{0}$ are given, and the solution maps for the Riccati ODEs (9a)-(9b) can be represented [24, p. 156], [25] as linear fractional transforms (LFTs), it is natural to speculate if (9) can be solved via a recursive algorithm, thereby solving (6). To do so, we need to construct mappings $\boldsymbol{P}_1 \mapsto \boldsymbol{P}_0$, $\boldsymbol{H}_0 \mapsto \boldsymbol{H}_1$, $\boldsymbol{H}_1 \mapsto \boldsymbol{P}_1$, where the subscript zero corresponds to $t = t_0$, and the subscript one corresponds to $t = t_1$. These mappings are to be constructed in a way that ensures invertibility of $\boldsymbol{P}_1 + \boldsymbol{\Sigma}_d$ in (9d).

In the next Sec. III, we propose the constructions for these maps and summarize the key structural properties of the matrix-valued mappings that underpin the proposed recursive algorithm. Detailed proofs are provided in [17].The results from Sec. III will be used for the design and analysis of the proposed algorithm in Sec. IV.

III. Construction of Matrix-valued Mappings

A. Mappings $\boldsymbol{P}_1 \mapsto \boldsymbol{P}_0, \boldsymbol{H}_0 \mapsto \boldsymbol{H}_1$

Let us denote the $2n \times 2n$ Hamiltonian matrix of the system as

$$\boldsymbol{M}_t := \begin{bmatrix} \boldsymbol{A}_t & -\boldsymbol{B}_t \boldsymbol{B}_t^\top \\ -\boldsymbol{Q}_t & -\boldsymbol{A}_t^\top \end{bmatrix}, \tag{10}$$

and its state transition matrix in block-partitioned form:

$$\boldsymbol{\Phi}(s,t) := \begin{bmatrix} \boldsymbol{\Phi}_{11}(s,t) & \boldsymbol{\Phi}_{12}(s,t) \\ \boldsymbol{\Phi}_{21}(s,t) & \boldsymbol{\Phi}_{22}(s,t) \end{bmatrix}, \quad t_0 \le s \le t \le t_1, \tag{11}$$

where $\boldsymbol{\Phi}_{ij}(s,t) \in \mathbb{R}^{n\times n}$ $\forall (i,j) \in \{1,2\}^2$. By definition,

$$\partial_t \boldsymbol{\Phi}(s,t) = \boldsymbol{M}(t)\boldsymbol{\Phi}(s,t), \quad \boldsymbol{\Phi}(s,s) = \boldsymbol{I}. \tag{12}$$

For convenience, consider slightly abused notation:

$$\begin{bmatrix} \boldsymbol{\Phi}_{11} & \boldsymbol{\Phi}_{12} \\ \boldsymbol{\Phi}_{21} & \boldsymbol{\Phi}_{22} \end{bmatrix} := \begin{bmatrix} \boldsymbol{\Phi}_{11}(t_0, t_1) & \boldsymbol{\Phi}_{12}(t_0, t_1) \\ \boldsymbol{\Phi}_{21}(t_0, t_1) & \boldsymbol{\Phi}_{22}(t_0, t_1) \end{bmatrix}. \tag{13}$$

The mapping $\boldsymbol{P}_1 \mapsto \boldsymbol{P}_0$ is the solution of the Riccati matrix ODE initial value problem (9a) backward in time from $t = t_1$ to $t = t_0$, with $\boldsymbol{P}_t(t = t_1) = \boldsymbol{P}_1 \in \mathbb{S}^n$ given. As is well-known [24, p. 156], [25], this mapping is an LFT in terms of the blocks of (13):

$$\boldsymbol{P}_0 = \left(\boldsymbol{P}_1\boldsymbol{\Phi}_{12} - \boldsymbol{\Phi}_{22}\right)^{-1}\left(\boldsymbol{\Phi}_{21} - \boldsymbol{P}_1\boldsymbol{\Phi}_{11}\right). \tag{14}$$

Thus, (14) is the explicit form for the mapping $\boldsymbol{P}_1 \mapsto \boldsymbol{P}_0$.

Likewise, the mapping $\boldsymbol{H}_0 \mapsto \boldsymbol{H}_1$ is the solution of the Riccati matrix ODE initial value problem (9b) forward in time from $t = t_0$ to $t = t_1$, with $\boldsymbol{H}_t(t = t_0) = \boldsymbol{H}_0 \in \mathbb{S}^n$ given. The counterpart of (14) is

$$\boldsymbol{H}_1 = -\left(\boldsymbol{\Phi}_{11}^\top - \boldsymbol{H}_0\boldsymbol{\Phi}_{12}^\top\right)^{-1}\left(\boldsymbol{\Phi}_{21}^\top - \boldsymbol{H}_0\boldsymbol{\Phi}_{22}^\top\right). \tag{15}$$

Thus, (15) is the explicit form for the mapping $\boldsymbol{H}_0 \mapsto \boldsymbol{H}_1$.

The principal structural result (established via [17, Theorem 1]) about the mappings $\boldsymbol{P}_1 \mapsto \boldsymbol{P}_0$ and $\boldsymbol{H}_0 \mapsto \boldsymbol{H}_1$ given by (14) and (15) respectively, is that they both are bijective and they take symmetric matrices to symmetric matrices.

B. Mapping $\boldsymbol{H}_1 \mapsto \boldsymbol{P}_1$

We start by noticing that (9d), or equivalently (6d) and (8) can be recast in the following two ways:

$$\boldsymbol{I} = \boldsymbol{\Sigma}_1\left(\boldsymbol{P}_1 + \boldsymbol{H}_1\right) = \left(\boldsymbol{P}_1 + \boldsymbol{\Sigma}_d\right)\left(\boldsymbol{P}_1 + \boldsymbol{H}_1\right), \tag{16}$$

$$\boldsymbol{I} = \left(\boldsymbol{P}_1 + \boldsymbol{H}_1\right)\boldsymbol{\Sigma}_1 = \left(\boldsymbol{P}_1 + \boldsymbol{H}_1\right)\left(\boldsymbol{P}_1 + \boldsymbol{\Sigma}_d\right), \tag{17}$$

wherein $\boldsymbol{I}$ denotes the identity matrix.

The equations (16)-(17) can be equivalently written as

$$\boldsymbol{P}_1^2 + \boldsymbol{P}_1\boldsymbol{H}_1 + \boldsymbol{\Sigma}_d\boldsymbol{P}_1 + \left(\boldsymbol{\Sigma}_d\boldsymbol{H}_1 - \boldsymbol{I}\right) = \boldsymbol{0}, \tag{18}$$

$$\boldsymbol{P}_1^2 + \boldsymbol{P}_1\boldsymbol{\Sigma}_d + \boldsymbol{H}_1\boldsymbol{P}_1 + \left(\boldsymbol{H}_1\boldsymbol{\Sigma}_d - \boldsymbol{I}\right) = \boldsymbol{0}. \tag{19}$$

The structures of (18) and (19) reveal the following: if either (18) or (19) admits a *symmetric* solution $\boldsymbol{P}_1$, that solution must satisfy both (18) and (19). So in effect, we have one algebraic equation in one symmetric unknown $\boldsymbol{P}_1$.

Now the question becomes whether (18) or (19), or some equivalent version of either, is more convenient for the mapping $\boldsymbol{H}_1 \mapsto \boldsymbol{P}_1$. One particularly simple equivalent version is obtained by subtracting (19) from (18), giving the Sylvester equation

$$\left(\boldsymbol{H}_1 - \boldsymbol{\Sigma}_d\right)\boldsymbol{P}_1 + \boldsymbol{P}_1\left(\boldsymbol{\Sigma}_d - \boldsymbol{H}_1\right) = \boldsymbol{\Sigma}_d\boldsymbol{H}_1 - \boldsymbol{H}_1\boldsymbol{\Sigma}_d. \tag{20}$$

In [17, Theorem 2], we establish that for any symmetric $\boldsymbol{H}_1$ and $\boldsymbol{\Sigma}_d \succ \boldsymbol{0}$, the Sylvester equation (20) possesses non-unique symmetric solutions $\boldsymbol{P}_1 = \boldsymbol{P}_1^\top$ and it is unclear which of the non-unique symmetric solutions can be used for the mapping $\boldsymbol{H}_1 \mapsto \boldsymbol{P}_1$, that can in turn guarantee convergence of the recursive algorithm. This analysis suggests that instead of removing the nonlinearity from (18)-(19), we should try to leverage the same.

As an alternative to (20), adding (18) and (19) gives an instance of Continuous-time Algebraic Riccati Equation (CARE):

$$\boldsymbol{P}_1^2 + \boldsymbol{P}_1\left(\frac{\boldsymbol{H}_1 + \boldsymbol{\Sigma}_d}{2}\right) + \left(\frac{\boldsymbol{H}_1 + \boldsymbol{\Sigma}_d}{2}\right)\boldsymbol{P}_1 + \left(\frac{\boldsymbol{\Sigma}_d\boldsymbol{H}_1 + \boldsymbol{H}_1\boldsymbol{\Sigma}_d}{2} - \boldsymbol{I}\right) = \boldsymbol{0}. \tag{21}$$

The principal structural result about the mapping $\boldsymbol{H}_1 \mapsto \boldsymbol{P}_1$ concerns the continuous-time algebraic Riccati equation (21). [17, Theorem 3] establishes that for any symmetric $\boldsymbol{H}_1$ and $\boldsymbol{\Sigma}_d \succ \boldsymbol{0}$, the CARE (21) admits non-unique symmetric solutions $\boldsymbol{P}_1 = \boldsymbol{P}_1^\top$. Among these symmetric solutions, however, there exists a unique stabilizing solution, given by

$$\boldsymbol{P}_1 = -\frac{\boldsymbol{H}_1 + \boldsymbol{\Sigma}_d}{2} + \left(\left(\frac{\boldsymbol{H}_1 - \boldsymbol{\Sigma}_d}{2}\right)^2 + \boldsymbol{I}\right)^{\frac{1}{2}}. \tag{22}$$

In [17, Theorem 3], we show that requiring stabilizability is a way to extract *unique* symmetric solution of the CARE (21). Furthermore, [17, Proposition 3] ensures the invertibility of $\boldsymbol{P}_1 + \boldsymbol{\Sigma}_d$ in (9d), where $\boldsymbol{P}_1$ is the unique stabilizing solution 21. In Sec. IV, we will use this stabilizing symmetric solution (22) for the mapping $\boldsymbol{H}_1 \mapsto \boldsymbol{P}_1$ and prove that this choice guarantees convergence of the recursive algorithm proposed in Sec. IV.

IV. Recursive Algorithm

Building on the results from Sec. II and III, we propose a fixed point recursion of the form $\boldsymbol{P}_0 \mapsto (\boldsymbol{P}_0)_{\text{next}}$ to solve (6). The proposed recursion, shown in Fig. 1, is a composition of four mappings:

- $\boldsymbol{P}_0 \to \boldsymbol{H}_0$ by evaluating (9c),
- $\boldsymbol{H}_0 \to \boldsymbol{H}_1$ by evaluating (15),
- $\boldsymbol{H}_1 \to \boldsymbol{P}_1$ by evaluating (22),
- $\boldsymbol{P}_1 \to (\boldsymbol{P}_0)_{\text{next}}$ by evaluating (14).

Notice that all four mappings above, and thus their composition, are guaranteed to map $\mathbb{S}^n \to \mathbb{S}^n$. So it suffices to perform the proposed recursion over the half-vectorization of $\boldsymbol{P}_0$, i.e., over $n(n+1)/2$ reals instead of n^2 reals. This is computationally helpful for large n. The proposed algorithm is a nonlinear recursion over the space of symmetric matrices. This recursion of the form $\boldsymbol{X} \mapsto \boldsymbol{F}(\boldsymbol{X})$, $\boldsymbol{X} \in \mathbb{S}^n$, where the matricial map $\boldsymbol{F} : \mathbb{S}^n \to \mathbb{S}^n$. Our main result is Theorem 1 that builds on auxiliary lemmas [17, Lemma 2-4] and establishes the existence-uniqueness of the fixed point $\boldsymbol{X}^\star \in \mathbb{S}^n$ of the proposed recursion, and its convergence. A natural proof strategy for such a result would be to show that the proposed recursion is contractive over the affine set $\mathbb{S}^n$ w.r.t. some metric such as the Frobenius or spectral norm of the difference. However, numerical experiments confirm that such contractive property does not hold for the proposed recursion $\boldsymbol{X} \mapsto \boldsymbol{F}(\boldsymbol{X})$. Another strategy could be separately arguing the existence-uniqueness of fixed point, and then establish the convergence by considering the function $V : \mathbb{S}^n \mapsto \mathbb{R}_{\geq 0}$ given by $V(\boldsymbol{X}) := \|\boldsymbol{X} - \boldsymbol{X}^\star\|^2_{\text{Frobenius}} = \text{trace}\,(\boldsymbol{X} - \boldsymbol{X}^\star)^2$ as a candidate Lyapunov function. However, numerics show that $V(\boldsymbol{F}(\boldsymbol{X})) \not< V(\boldsymbol{X})$ for all $\boldsymbol{X} \in \mathbb{S}^n \setminus \{\boldsymbol{X}^\star\}$. It is also unclear what could be an alternative choice of candidate Lyapunov function. Last but not the least, it is not apparent how to handle possible non-existence of inverses appearing in the LFTs (14)-(15). Due to these difficulties, the proposed recursion calls for a careful reasoning.

Theorem 1. *Given the state transition matrix* (11) *associated with* (10)*, and* $\boldsymbol{\Sigma}_0, \boldsymbol{\Sigma}_d \in \mathbb{S}^n_{++}$*, define the mappings*

$$\boldsymbol{F}_1(\boldsymbol{X}) := \boldsymbol{\Sigma}_0^{-1} - \boldsymbol{X}, \tag{23a}$$

$$\boldsymbol{F}_2(\boldsymbol{X}) := -\left(\boldsymbol{\Phi}_{11}^\top - \boldsymbol{X}\boldsymbol{\Phi}_{12}^\top\right)^{-1}\left(\boldsymbol{\Phi}_{21}^\top - \boldsymbol{X}\boldsymbol{\Phi}_{22}^\top\right), \tag{23b}$$

$$\boldsymbol{F}_3(\boldsymbol{X}) := -\frac{\boldsymbol{X} + \boldsymbol{\Sigma}_d}{2} + \left(\left(\frac{\boldsymbol{X} - \boldsymbol{\Sigma}_d}{2}\right)^2 + \boldsymbol{I}\right)^{\frac{1}{2}}, \tag{23c}$$

$$\boldsymbol{F}_4(\boldsymbol{X}) := \left(\boldsymbol{X}\boldsymbol{\Phi}_{12} - \boldsymbol{\Phi}_{22}\right)^{-1}\left(\boldsymbol{\Phi}_{21} - \boldsymbol{X}\boldsymbol{\Phi}_{11}\right), \tag{23d}$$

in variable $\boldsymbol{X} \in \mathbb{S}^n$*. The square root in* (23c) *is understood as the principal square root. Then*

- *the composite endomorphism* $\boldsymbol{F} := \boldsymbol{F}_4 \circ \boldsymbol{F}_3 \circ \boldsymbol{F}_2 \circ \boldsymbol{F}_1$ *that maps* $\mathbb{S}^n \to \mathbb{S}^n$*, has a unique fixed point,*
- *the recursion* $\boldsymbol{P}_0 \mapsto (\boldsymbol{P}_0)_{next} = \boldsymbol{F}(\boldsymbol{P}_0)$ *converges to this unique fixed point for almost every* $\boldsymbol{P}_0 \in \mathbb{S}^n$*.*

Proof. **Existence-uniqueness of fixed point.** From [Theorem 1] [17], the LFTs (23b)-(23d), in their domain of definitions, are bijective. So is the linear map (23a). Since $(\boldsymbol{X} - \boldsymbol{\Sigma}_d)/2$ is symmetric, its square is positive semidefinite (by spectral theorem), so the square root in (23c) acts on a positive definite matrix. Because principal square root is bijective over the positive semidefinite cone, the mapping (23c) is also bijective. As a result, the composition $\boldsymbol{F} := \boldsymbol{F}_4 \circ \boldsymbol{F}_3 \circ \boldsymbol{F}_2 \circ \boldsymbol{F}_1$ is bijective. Hence $\boldsymbol{F}$ can have *at most one* fixed point.

Now we argue that $\boldsymbol{F}$ has *at least one* fixed point. To do so, we note that the set $\mathbb{S}^n$ is closed and convex (w.r.t. standard Euclidean norm topology). The composite map $\boldsymbol{F} : \mathbb{S}^n \to \mathbb{S}^n$ is continuous and bounded. This can be seen from the fact that by [17, Lemma 2], the map $\boldsymbol{F}_4$ is bounded, and by similar argument, $\boldsymbol{F}_2$ is bounded as well. The map $\boldsymbol{F}_1$, being affine, is non-expansive. By [17, Lemma 3], the map $\boldsymbol{F}_3$ is non-expansive as well. Finally, the $\boldsymbol{F}_i$ are continuous for all $i = 1, \ldots, 4$. So for any $\boldsymbol{X} \in \mathbb{S}^n$ with finite norm, the half-vectorization map $\boldsymbol{f} := \text{vech}(\boldsymbol{F}(\boldsymbol{X})) : \mathbb{R}^{n(n+1)/2} \to \mathbb{R}^{n(n+1)/2}$ is uniformly bounded by some finite $M > 0$, i.e.,

$$\sup_{i \in \{1, \ldots, \frac{n(n+1)}{2}\}} \sup_{\boldsymbol{x} \in \mathbb{R}^{\frac{n(n+1)}{2}}} |f_i(\boldsymbol{x})| \leq M. \tag{24}$$

Algorithm 1 Solve LQ covariance steering problem (1) with terminal cost (2)

Require: Time horizon $[t_0, t_1]$, matrix tuple $(\boldsymbol{A}_t, \boldsymbol{B}_t, \boldsymbol{Q}_t)\ \forall t \in [t_0, t_1]$ satisfying assumptions **A1**-**A2**, covariances $\boldsymbol{\Sigma}_0, \boldsymbol{\Sigma}_d$ satisfying assumption **A3**, numerical tolerance `tol`, maximum number of iteration `maxIter`

1: Compute the state transition matrix (13) for the coefficient matrix (10)
2: Make a random initial guess $\boldsymbol{P}_0 \in \mathbb{S}^n$ ▷ i.i.d. uniform $n(n+1)/2$ entries over some bounding box
3: `err` $\leftarrow 0$ ▷ Initialize error
4: `idx` $\leftarrow 1$ ▷ Initialize recursion index
5: **while** ((`err`>`tol`)&&(`idx`≤`maxIter`)) **do**
6: $\quad \boldsymbol{H}_0 \leftarrow \boldsymbol{\Sigma}_0^{-1} - \boldsymbol{P}_0$ ▷ From (9c)
7: $\quad \boldsymbol{H}_1 \leftarrow \left(\boldsymbol{H}_0\boldsymbol{\Phi}_{12}^\top - \boldsymbol{\Phi}_{11}^\top\right)^{-1}\left(\boldsymbol{\Phi}_{21}^\top - \boldsymbol{H}_0\boldsymbol{\Phi}_{22}^\top\right)$ ▷ From (15)
8: $\quad \boldsymbol{P}_1 \leftarrow -\frac{\boldsymbol{H}_1+\boldsymbol{\Sigma}_d}{2} + \left(\left(\frac{\boldsymbol{H}_1-\boldsymbol{\Sigma}_d}{2}\right)^2 + \boldsymbol{I}\right)^{\frac{1}{2}}$ ▷ From (22)
9: $\quad (\boldsymbol{P}_0)_{\text{next}} \leftarrow (\boldsymbol{P}_1\boldsymbol{\Phi}_{12} - \boldsymbol{\Phi}_{22})^{-1}(\boldsymbol{\Phi}_{21} - \boldsymbol{P}_1\boldsymbol{\Phi}_{11})$ ▷ From (14)
10: $\quad$ `err` $\leftarrow \|\,(\boldsymbol{P}_0)_{\text{next}} - \boldsymbol{P}_0\|_{\text{Frobenius}}$ ▷ Update error
11: $\quad$ `idx` $\leftarrow$ `idx` $+ 1$ ▷ Update recursion index
12: $\quad \boldsymbol{P}_0 \leftarrow (\boldsymbol{P}_0)_{\text{next}}$
13: **end while**
14: $\boldsymbol{P}_t^{\text{opt}}\ \forall t \in [t_0, t_1] \leftarrow$ integrate (6b) with converged $\boldsymbol{P}_0$ as initial condition
15: $\boldsymbol{\Sigma}_t^{\text{opt}}\ \forall t \in [t_0, t_1] \leftarrow$ integrate (6a) with $\boldsymbol{\Sigma}_0$ as initial condition, and computed $\boldsymbol{P}_t^{\text{opt}}$ ▷ Optimally controlled covariance
16: $\boldsymbol{K}_t^{\text{opt}} \leftarrow -\boldsymbol{B}_t^\top \boldsymbol{P}_t^{\text{opt}}\ \forall t \in [t_0, t_1]$ ▷ Optimal feedback gain
17: **return** $\boldsymbol{\Sigma}_t^{\text{opt}}, \boldsymbol{K}_t^{\text{opt}}\ \forall t \in [t_0, t_1]$

Hence $\boldsymbol{f}$ maps the compact convex set $[-M, M]^{n(n+1)/2}$ to itself. By Brouwer's fixed point theorem [26, p. 14], $\boldsymbol{f}$ and thus $\boldsymbol{F}$, admits a fixed point.

Combining the "at most one" and "at least one" arguments, we conclude that the map $\boldsymbol{F}$ has a unique fixed point.

Convergence. To set aside the issue of possible initial conditions $\boldsymbol{X}^{(0)} \in \mathbb{S}^n$ for which the inverses in the LFTs (23b), (23d) may not exist during the recursion, consider for now only those $\boldsymbol{X}^{(0)} \in \mathbb{S}^n$ for which $\{\boldsymbol{X}^{(k)}\}_{k\in\mathbb{N}}$ remains a well-defined sequence of real symmetric matrices generated by $\boldsymbol{X}^{(k)} = \boldsymbol{F}^{(k)}(\boldsymbol{X}^{(0)})$, where $\boldsymbol{F}^{(k)}$ denotes k-fold composition of $\boldsymbol{F}$. Call such initial conditions as "good" $\boldsymbol{X}^{(0)} \in \mathbb{S}^n$. We will address its complement, i.e., "bad" $\boldsymbol{X}^0 \in \mathbb{S}^n$ leading to LFT singularity in a bit.

By (24), the sequence $\{\boldsymbol{X}^{(k)}\}_{k\in\mathbb{N}}$ generated by "good" $\boldsymbol{X}^0$, is bounded, and therefore, by the Bolzano-Weierstrass theorem [27, Thm. 3.6(b)], has a convergent subsequence. Since $\mathbb{S}^n$ is closed, the limit point of the convergent subsequence must also be in $\mathbb{S}^n$. Furthermore, by continuity of $\boldsymbol{F}$, this limit point must be a fixed point of the map $\boldsymbol{X} \mapsto \boldsymbol{F}(\boldsymbol{X})$. On the other hand, we already proved the existence-uniqueness of fixed point for $\boldsymbol{F} : \mathbb{S}^n \to \mathbb{S}^n$. So the full sequence $\{\boldsymbol{X}^{(k)}\}$ converges to the same fixed point (since otherwise, we could extract a subsequence bounded away from this fixed point, which would converge to a different limit point, contradicting uniqueness). This proves that convergence to unique fixed point is guaranteed for all "good" $\boldsymbol{X}^{(0)} \in \mathbb{S}^n$.

Now let us address a "bad" $\boldsymbol{X}^{(0)} \in \mathbb{S}^n$ that leads to singularity in any of the two LFTs (23b), (23d). Notice that both these LFTs are of the form $(\boldsymbol{R} - \boldsymbol{X}\boldsymbol{S})^{-1}\left(\boldsymbol{X}\tilde{\boldsymbol{R}} - \tilde{\boldsymbol{S}}\right)$ with $\boldsymbol{R} = \boldsymbol{\Phi}_{11}^\top$, $\boldsymbol{S} = \boldsymbol{\Phi}_{11}^\top$ for (23b), and $\boldsymbol{R} = \boldsymbol{\Phi}_{22}$, $\boldsymbol{S} = \boldsymbol{\Phi}_{12}$ for (23d). From [17, Lemma 4], the wide matrix $[\boldsymbol{R}, -\boldsymbol{S}]$ is nondegenerate ([17, Definition 1]) for both (23b) and (23d). By [28, Thm. 1], for $[\boldsymbol{R}, -\boldsymbol{S}]$ nondegenerate, the collection of $\boldsymbol{X} \in \mathbb{S}^n$ such that $\boldsymbol{R} - \boldsymbol{X}\boldsymbol{S}$ is nonsingular is dense in $\mathbb{S}^n$. Thus, the collection of "bad" $\boldsymbol{X}^{(0)} \in \mathbb{S}^n$ is a set of measure zero, i.e., convergence to unique fixed point is guaranteed for almost every $\boldsymbol{X}^{(0)} \in \mathbb{S}^n$. ■

Algorithm 1 outlines the overall computation. We stress here the importance of random initial guess stated in line 2 of Algorithm 1. Since the convergence guarantee in Theorem 1 holds for almost every $\boldsymbol{P}_0 \in \mathbb{S}^n$, Algorithm 1 converges in practice (i.e., with probability one). Our numerical example presented in Sec. V next, find that the convergence is fast in practice.

V. Noisy Clohessy-Wiltshire Model

In this Section, we illustrate the effectiveness of the proposed covariance steering algorithm via a numerical example. We fix $[t_0, t_1] = [0, 1]$. To implement the recursion $\boldsymbol{P}_0 \mapsto (\boldsymbol{P}_0)_{\text{next}}$, we use `while` loop with convergence criterion that all components of $\boldsymbol{P}_0$ and $(\boldsymbol{P}_0)_{\text{next}}$ are within an absolute deviation (i.e., numerical tolerance) of 10^{-8} or less.

We consider a close-proximity orbital rendezvous dynamics depicted in Fig. 2 where a service spacecraft (hereafter "chaser") is dispatched from a nearby parking orbit to inspect a satellite (hereafter "target") located in a circular Low-Earth Orbit (LEO) at an altitude of 415.137 km. As standard, we denote the relative 3D position vector of the chaser w.r.t. the target as $x\boldsymbol{i}_r + y\boldsymbol{i}_\theta + z\boldsymbol{i}_z$, where the unit vector $\boldsymbol{i}_r$ points in radially outward direction from the target satellite, $\boldsymbol{i}_\theta$ is along the direction of motion of the target satellite, and $\boldsymbol{i}_z$ is normal to the orbital plane.

The noisy version of the Clohessy-Wiltshire equation [29] models the linearized relative dynamics of the chaser w.r.t. the target. This model has $n = 6$ states, $m = 3$ inputs and noises, and is the following instance of (1b):

$$\mathrm{d}x_{1t} = x_{2t}\,\mathrm{d}t, \tag{25a}$$
$$\mathrm{d}x_{2t} = \left(3\nu^2 x_{1t} + 2\nu x_{4t} + u_{1t}\right)\mathrm{d}t + \mathrm{d}w_{1t}, \tag{25b}$$
$$\mathrm{d}x_{3t} = x_{4t}\,\mathrm{d}t, \tag{25c}$$
$$\mathrm{d}x_{4t} = (-2\nu x_{2t} + u_{2t})\,\mathrm{d}t + \mathrm{d}w_{2t}, \tag{25d}$$
$$\mathrm{d}x_{5t} = x_{6t}\,\mathrm{d}t, \tag{25e}$$
$$\mathrm{d}x_{6t} = \left(-\nu^2 x_{5t} + u_{3t}\right)\mathrm{d}t + \mathrm{d}w_{3t}, \tag{25f}$$

where $(x_{1t}, x_{3t}, x_{5t}) \equiv (x, y, z)$ are the relative position coordinates explained earlier, (x_{2t}, x_{4t}, x_{6t}) are the relative velocity coordinates, and (u_{1t}, u_{2t}, u_{3t}) are the thruster acceleration inputs. The standard Wiener processes (w_{1t}, w_{2t}, w_{3t}) in (25) model process noise such as thruster actuation noise, solar radiation pressure, along the acceleration channels.

In (25), the parameter $\nu := \sqrt{\mu/a^3} = 1.1276 \times 10^{-3}$ rad/s is the constant orbital rate of the target, $\mu = 3.9860 \times 10^{14}$ m^3/s^2 is the standard gravitational parameter of the Earth, and $a = 6793.237$ Km is the radius of the circular LEO in which the target resides.

Let

$$\boldsymbol{A}^{(1)} := \nu^2\,[3\boldsymbol{e}_1|\boldsymbol{0}_{3\times1}| - \boldsymbol{e}_3]\,, \quad \boldsymbol{A}^{(2)} := \nu\,[-2\boldsymbol{e}_2|2\boldsymbol{e}_3|\boldsymbol{0}_{3\times1}]\,,$$

where $\{\boldsymbol{e}_i\}_{i=1,2,3}$ are the standard basis column vectors in $\mathbb{R}^3$. It is easy to verify that the system matrix pair for (25):

$$(\boldsymbol{A}_t, \boldsymbol{B}_t) \equiv \left(\begin{bmatrix} \boldsymbol{0}_{3\times3} & \boldsymbol{I}_{3\times3} \\ \boldsymbol{A}^{(1)} & \boldsymbol{A}^{(2)} \end{bmatrix}, \begin{bmatrix} \boldsymbol{0}_{3\times3} \\ \boldsymbol{I}_{3\times3} \end{bmatrix}\right) \quad \forall t \in [t_0, t_1],$$

satisfies assumption **A1**. Since covariance steering is decoupled from the mean steering (see [17, Remark 1]), we focus on steering the initial joint state PDF $\rho_0 = \mathcal{N}(\boldsymbol{0}, \boldsymbol{\Sigma}_0)$ close to the desired joint state PDF $\rho_d = \mathcal{N}(\boldsymbol{0}, \boldsymbol{\Sigma}_d)$. We fix $\boldsymbol{Q} = \boldsymbol{I}$,

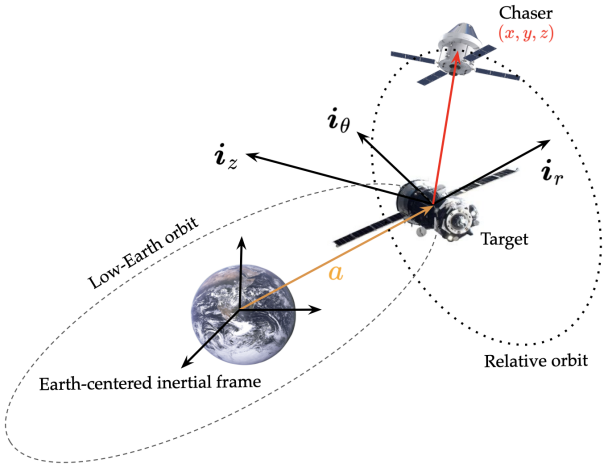

Fig. 2 The relative orbital dynamics for the noisy Clohessy–Wiltshire model in Sec. V.

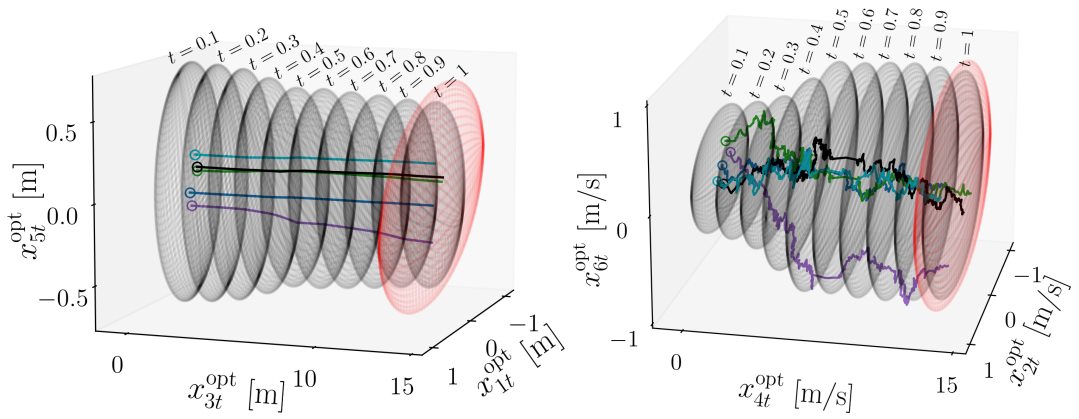

(a) Marginal position covariances. **(b) Marginal velocity covariances.**

Fig. 3 Optimally controlled covariances (gray wireframe ellipsoids) and 5 closed-loop state sample paths for the noisy CW model in the (a) position and (b) velocity coordinates. The hollow circular markers denote the initial conditions for these sample paths. The red wireframe ellipsoids correspond to the position and velocity marginal covariances of $\mathbf{\Sigma}_d$.

and use randomly generated positive definite

$$\mathbf{\Sigma}_0 = \begin{bmatrix} 5.9148 & 3.8100 & 2.5815 & 2.1795 & 4.1628 & 1.9270 \\ 3.8100 & 5.5664 & 2.8501 & 2.1819 & 3.8496 & 3.3638 \\ 2.5815 & 2.8501 & 3.3834 & 1.5591 & 2.5389 & 2.3088 \\ 2.1795 & 2.1819 & 1.5591 & 3.5850 & 2.6187 & 2.0098 \\ 4.1628 & 3.8496 & 2.5389 & 2.6187 & 5.1285 & 2.5639 \\ 1.9270 & 3.3638 & 2.3088 & 2.0098 & 2.5639 & 5.4354 \end{bmatrix}, \mathbf{\Sigma}_d = \begin{bmatrix} 1.6431 & 1.1138 & 1.5453 & 1.1729 & 1.2916 & 0.4077 \\ 1.1138 & 1.9581 & 1.4418 & 1.0926 & 1.2408 & 0.4495 \\ 1.5453 & 1.4418 & 3.9142 & 1.9928 & 2.0221 & 1.5553 \\ 1.1729 & 1.0926 & 1.9928 & 2.1027 & 1.3448 & 0.9645 \\ 1.2916 & 1.2408 & 2.0221 & 1.3448 & 1.7077 & 0.7830 \\ 0.4077 & 0.4495 & 1.5553 & 0.9645 & 0.7830 & 1.5008 \end{bmatrix},$$

thereby satisfying assumptions **A2**-**A3**.

Fig. 4a shows convergence of the recursion $\boldsymbol{P}_0 \mapsto (\boldsymbol{P}_0)_{\text{next}}$ proposed in Sec. IV with randomly initialized $\boldsymbol{P}_0 \in \mathbb{S}^6$. Fig. 3 plots the marginal 1σ covariance ellipsoids in the position (Fig. 3(a)) and velocity (Fig. 3(b)) coordinates[‡], along with 5 closed-loop sample paths w.r.t. time $t \in [0, 1]$. As in the previous example, the initial conditions for these 5 paths are sampled from the six dimensional Gaussian ρ_0, and the paths are obtained by the Euler-Maruyama integration with the same step size as before. In Fig. 3, the closed-loop position trajectories have more fluctuations than the closed-loop velocity trajectories, which is expected since (25) is a degenerate Itô diffusion.In Fig. 3, we indicate the directionality of time by spatially translating the centers of the covariance ellipsoids along the y position and velocity coordinate, respectively. In each subfigure, an ellipsoid represents a specific covariance snapshot.

The terminal covariance resulting from our controller is

$$\mathbf{\Sigma}_1 = \begin{bmatrix} 4.4809 & 3.1131 & 2.3911 & 0.4248 & 0.5287 & 0.0363 \\ 3.1131 & 5.0291 & 3.0649 & 0.2636 & 0.4523 & 0.0130 \\ 2.3911 & 3.0649 & 5.1735 & 1.3626 & 1.0944 & 1.2781 \\ 0.4248 & 0.2636 & 1.3626 & 2.3281 & 1.2304 & 1.0207 \\ 0.5287 & 0.4523 & 1.0944 & 1.2304 & 1.8847 & 0.8106 \\ 0.0363 & 0.0130 & 1.2781 & 1.0207 & 0.8106 & 1.7013 \end{bmatrix}$$

which is close to the desired, as seen in Fig. 3.

Fig. 4b shows the optimal input sample paths corresponding to the closed-loop state sample paths in Fig. 3.

[‡]Recall that the covariance of the marginal of a Gaussian joint distribution is simply the corresponding submatrix of the original covariance matrix.

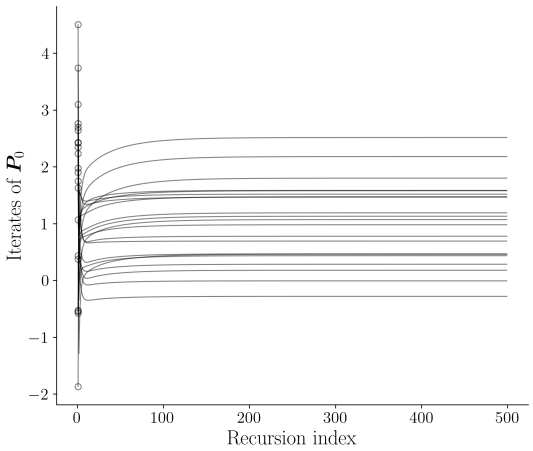

(a) Convergence of the 21 triangular elements of $P_0 \in \mathbb{S}^6$ for the noisy CW model. The random initializations are shown as hollow circular markers.

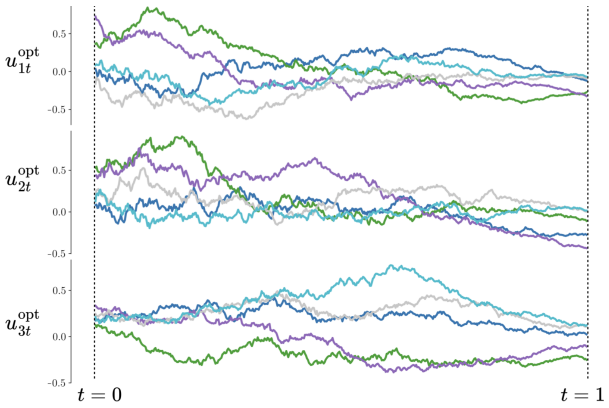

(b) Sample paths for the optimal inputs (in m/s^2) corresponding to the state sample paths in Fig. 3.

VI. Concluding Remarks

We formulated and solved the fixed-horizon linear-quadratic covariance steering problem in continuous time, where the terminal cost is measured by the Hilbert-Schmidt (i.e., Frobenius) norm error between the desired and controlled terminal covariances. The optimality conditions were derived and recast as a coupled Riccati-Riccati system of matrix ODEs. Leveraging the linear fractional transforms associated with the solution maps of these ODEs and their structural properties, we proposed a novel matrix-valued nonlinear recursion on the space of symmetric matrices to solve the optimality conditions, and proved its convergence to a unique fixed point. The optimal control and the optimally controlled covariance were computed for a close-proximity orbital rendezvous scenario using the noisy Clohessy-Wiltshire model, with numerical results confirming fast convergence in practice and validating the computational feasibility of the proposed approach.

Several extensions of the present work are worth noting. The problem formulation and the proposed algorithm extend in a straightforward manner to a weighted terminal cost of the form $\frac{1}{2}\|\boldsymbol{W}^{\frac{1}{2}}\,(\boldsymbol{\Sigma}_1 - \boldsymbol{\Sigma}_d)\,\|^2_{\text{Frobenius}}$ for a fixed positive definite weight matrix $\boldsymbol{W}$, and also to the case where the Gaussian PDFs ρ_0, ρ_d have nonzero means (see [17, Remark 1]). A more compelling direction for future research is to investigate whether analogous matricial recursive algorithms with convergence guarantees can be designed for alternative terminal costs, such as the Bures-Wasserstein metric [6] between the controlled and desired terminal covariances. This will be pursued in future work.

Acknowledgments

This research was supported by NSF award 2111688.

References

[1] Hotz, A., and Skelton, R. E., "Covariance control theory," *International Journal of Control*, Vol. 46, No. 1, 1987, pp. 13–32.

[2] Zhu, G., Grigoriadis, K. M., and Skelton, R. E., "Covariance control design for Hubble space telescope," *Journal of Guidance, Control, and Dynamics*, Vol. 18, No. 2, 1995, pp. 230–236.

[3] Ridderhof, J., Pilipovsky, J., and Tsiotras, P., "Chance-constrained covariance control for low-thrust minimum-fuel trajectory optimization," *AAS/AIAA Astrodynamics Specialist Conference*, 2020, pp. 9–13.

[4] Benedikter, B., Zavoli, A., Wang, Z., Pizzurro, S., and Cavallini, E., "Convex approach to covariance control with application to stochastic low-thrust trajectory optimization," *Journal of Guidance, Control, and Dynamics*, Vol. 45, No. 11, 2022, pp. 2061–2075.

[5] Kumagai, N., and Oguri, K., "Sequential chance-constrained covariance steering for robust cislunar trajectory design under uncertainties," *AAS/AIAA Astrodynamics Specialist Conference*, 2024.

[6] Halder, A., and Wendel, E. D., "Finite horizon linear quadratic Gaussian density regulator with Wasserstein terminal cost," *2016 American Control Conference (ACC)*, IEEE, 2016, pp. 7249–7254.

[7] Bhatia, R., *Positive definite matrices*, Princeton university press, 2009.

[8] Balci, I. M., and Bakolas, E., "Covariance steering of discrete-time stochastic linear systems based on Wasserstein distance terminal cost," *IEEE Control Systems Letters*, Vol. 5, No. 6, 2020, pp. 2000–2005.

[9] Balci, I. M., Halder, A., and Bakolas, E., "On the convexity of discrete time covariance steering in stochastic linear systems with Wasserstein terminal cost," *2021 60th IEEE Conference on Decision and Control (CDC)*, IEEE, 2021, pp. 2318–2323.

[10] Yin, J., Zhang, Z., Theodorou, E., and Tsiotras, P., "Trajectory distribution control for model predictive path integral control using covariance steering," *2022 International Conference on Robotics and Automation (ICRA)*, IEEE, 2022, pp. 1478–1484.

[11] Saravanos, A. D., Balci, I. M., Bakolas, E., and Theodorou, E. A., "Distributed model predictive covariance steering," *2024 IEEE/RSJ International Conference on Intelligent Robots and Systems (IROS)*, IEEE, 2024, pp. 5740–5747.

[12] Morimoto, K., and Kashima, K., "Minimum energy density steering of linear systems with Gromov-Wasserstein terminal cost," *IEEE Control Systems Letters*, Vol. 8, 2024, pp. 586–591.

[13] Nakashima, H., Ganguly, S., Morimoto, K., and Kashima, K., "Formation Shape Control using the Gromov-Wasserstein Metric," *arXiv preprint arXiv:2503.21538*, 2025.

[14] Mémoli, F., "Gromov–Wasserstein distances and the metric approach to object matching," *Foundations of computational mathematics*, Vol. 11, No. 4, 2011, pp. 417–487.

[15] Salmona, A., Delon, J., and Desolneux, A., "Gromov-Wasserstein Distances between Gaussian Distributions," *Journal of Applied Probability*, Vol. 59, No. 4, 2022.

[16] Hoshino, K., "Finite-horizon optimal control of continuous-time stochastic systems with terminal cost of Wasserstein distance," *2023 62nd IEEE Conference on Decision and Control (CDC)*, IEEE, 2023, pp. 5825–5830.

[17] Sial, T., and Halder, A., "Fixed Horizon Linear Quadratic Covariance Steering in Continuous Time with Hilbert–Schmidt Terminal Cost," *arXiv preprint arXiv:2510.21944*, 2025.

[18] Bhatia, R., Jain, T., and Lim, Y., "On the Bures–Wasserstein distance between positive definite matrices," *Expositiones Mathematicae*, Vol. 37, No. 2, 2019, pp. 165–191.

[19] Givens, C. R., and Shortt, R. M., "A class of Wasserstein metrics for probability distributions." *Michigan Mathematical Journal*, Vol. 31, No. 2, 1984, pp. 231–240.

[20] Gelbrich, M., "On a formula for the L2 Wasserstein metric between measures on Euclidean and Hilbert spaces," *Mathematische Nachrichten*, Vol. 147, No. 1, 1990, pp. 185–203.

[21] Dowson, D., and Landau, B., "The Fréchet distance between multivariate normal distributions," *Journal of multivariate analysis*, Vol. 12, No. 3, 1982, pp. 450–455.

[22] Chen, Y., Georgiou, T., and Pavon, M., "Optimal steering of inertial particles diffusing anisotropically with losses," *2015 American Control Conference (ACC)*, IEEE, 2015, pp. 1252–1257.

[23] Chen, Y., Georgiou, T. T., and Pavon, M., "Optimal Steering of a Linear Stochastic System to a Final Probability Distribution—Part III," *IEEE Transactions on Automatic Control*, Vol. 63, No. 9, 2018, pp. 3112–3118. https://doi.org/10.1109/TAC.2018.2791362.

[24] Brockett, R. W., *Finite dimensional linear systems*, SIAM, 2015.

[25] Shayman, M. A., "Phase portrait of the matrix Riccati equation," *SIAM Journal on Control and Optimization*, Vol. 24, No. 1, 1986, pp. 1–65.

[26] Milnor, J. W., *Topology from the differentiable viewpoint*, Princeton University Press, Princeton, New Jersey, 1965.

[27] Rudin, W., *Principles of mathematical analysis*, 3rd ed., McGraw-Hill Science, 1976.

[28] Potapov, V., "Linear fractional transformations of matrices," *American Mathematical Society Translations: Series 2*, Vol. 138, 1988, pp. 21–35.

[29] Clohessy, W., and Wiltshire, R., "Terminal guidance system for satellite rendezvous," *Journal of the aerospace sciences*, Vol. 27, No. 9, 1960, pp. 653–658.